Lab on a Chip

PAPER

View Article Online
View Journal | View Issue

Cite this: *Lab Chip*, 2023, **23**, 1649

An integrated microfluidic chip for studying the effects of neurotransmitters on neurospheroids†

Subin Mao,‡[a] Catherine Fonder,‡[bcf] Md Fazlay Rubby,‡[a] Gregory J. Phillips,[ef] Donald S. Sakaguchi *[bcdf] and Long Que *[a]

To improve our understanding of how the central nervous system functions in health and disease, we report the development of an integrated chip for studying the effects of the neurotransmitters dopamine and serotonin on adult rat hippocampal progenitor cell (AHPC) neurospheroids. This chip allows dopamine or serotonin located in one chamber to diffuse to AHPC neurospheroids cultured in an adjacent chamber through a built-in diffusion barrier created by an array of intentionally misaligned micropillars. The gaps among the micropillars are filled with porous poly(ethylene glycol) (PEG) gel to tune the permeability of the diffusion barrier. An electrochemical sensor is also integrated within the chamber where the neurospheroids can be cultured, thereby allowing monitoring of the concentrations of dopamine or serotonin. Experiments show that concentrations of the neurotransmitters inside the neurospheroid chamber can be increased over a period of several hours to over 10 days by controlling the compositions of the PEG gel inside the diffusion barrier. The AHPC neurospheroids cultured in the chip remain highly viable following dopamine or serotonin treatment. Cell proliferation and neuronal differentiation have also been observed following treatment, revealing that the AHPC neurospheroids are a valuable *in vitro* brain model for neurogenesis research. Finally, we show that by tuning the permeability of diffusion barrier, we can block transfer of *Escherichia coli* cells across the diffusion barrier, while allowing dopamine or serotonin to pass through. These results suggest the feasibility of using the chip to better understand the interactions between microbiota and brain *via* the gut–brain axis.

Received 14th August 2022,
Accepted 31st January 2023

DOI: 10.1039/d2lc00755j

rsc.li/loc

1. Introduction

It is now known that new neurons can be continually generated in specific regions of the adult mammalian brain that become functionally integrated into existing neuronal networks.[1] Specifically, research has shown that mature cells in all neural lineages, including neurons, can be generated throughout adulthood in two distinct areas of the forebrain, the subventricular zone (SVZ) and the subgranular zone (SGZ) of the dentate gyrus of the hippocampus.[2] Within the brain, there are neural stem cells (NSCs) in specific microenvironments known as the stem cell niches. Injury or damage to the central nervous system (CNS) due to neurodegenerative diseases can result in the loss of specialized cells within these stem cell niches or surrounding tissues. Developing strategies for nervous system repair or regeneration of these specialized cells requires using directed differentiation techniques to guide stem cells towards specific neural lineages. Chemical induction techniques are common methods of guiding NSC differentiation.[3] Neurotransmitters can be one method to guide the differentiation of NSC towards specific neural lineages as it has been reported that neurotransmitters are not only associated with chemical communication between differentiated neurons but also provide critical components of the niche signals, thus modulating different aspects of neurogenesis.[4–7] The neurotransmitters dopamine and serotonin have been found to have positive effects on neurogenesis and proliferation within the CNS.[8–14] For instance, some research groups reported that the neurotransmitter dopamine plays a role in regulating endogenous neurogenesis in the adult mammalian brain such as in the ventricular–subventricular zone (V–SVZ).[9,15] The counter-regulatory interactions between the renin–angiotensin system and dopamine in peripheral tissues

[a] *Department of Electrical and Computer Engineering, Iowa State University, Ames IA 50011, USA. E-mail: lque@iastate.edu*
[b] *Molecular, Cellular, and Developmental Biology Program, Iowa State University, Ames IA 50011, USA. E-mail: dssakagu@iastate.edu*
[c] *Department of Genetics, Development and Cell Biology, Iowa State University, Ames IA 50011, USA*
[d] *Neuroscience Program, Iowa State University, Ames IA 50011, USA*
[e] *Department of Veterinary Microbiology, Iowa State University, Ames IA 50011, USA*
[f] *Nanovaccine Institute, Iowa State University, Ames IA 50011, USA*
† Electronic supplementary information (ESI) available. See DOI: **https://10.1039/d2lc00755j**
‡ Equal contribution.

and in the nigrostriatal system have been reported. However, the specific role of dopamine and the mechanisms underlying its effects on physiological and pathological conditions such as neurodegenerative diseases remain unclear.[15] Other research has suggested that the production of new neurons can be enhanced by serotonin through activating the 5HT1A receptor.[11] Substantial numbers of new granule neurons can be produced in the adult hippocampal formation, spanning the entire process across mammalian evolution. In general, it can be concluded that serotonin plays a direct regulatory role in activity-dependent hippocampal neurogenesis.[12]

Given these observations, along with other emerging paradigms in neuroscience, new experimental approaches are needed to improve our understanding how the CNS functions in health and disease. For example, to determine the function of the newly discovered types of neurons, it is important to identify the factors and conditions that regulate their occurrence. Furthermore, it remains controversial if neurogenesis exists *in vivo* in the adult mammalian substantia nigra, a midbrain dopaminergic nucleus.[15] Further studies therefore are needed to clarify how neurotransmitter signaling pathways control neurogenesis.[5,6,16] In the recent decades, most research efforts have utilized *in vivo* approaches to study possible neurogenesis due to neurotransmitter involvement.[6] While the *in vivo* studies are critical for reliable evaluation of the effects of neurotransmitters on neurogenesis, *in vitro* studies can provide some clear advantages, given their cost-effectiveness, quick turn-around time, without review and approval for animal use. Despite these advantages, to date there have been few efforts reported to study neurotransmitter activity using an *in vitro* brain model on-chip. In terms of *in vitro* brain model, many efforts have been devoted to developing *in vitro* brain models on chip in the past decades for different applications, including pathological studies, brain disease studies, and drug development,[17–24] just to name a few. However, as aforementioned, few efforts have been reported to evaluate the interactions between neurotransmitters and an *in vitro* brain model on-chip.

In response to this need, we report development of an integrated chip for studying the effects of neurotransmitters, including dopamine and serotonin, in combination with an *in vitro* brain model (*i.e.*, AHPC neurospheroids).[25,26] Specifically, to investigate the effect of the dopamine and serotonin neurotransmitters in the proliferation and differentiation of NSCs *in vitro*, adult rat hippocampal progenitor cells (AHPC) neurospheroids were used. AHPCs are a multipotent NSC population capable of differentiating into the three primary cell types of the CNS: neurons, oligodendrocytes, and astrocytes.[27] AHPCs are present within the adult mammalian brain and have been shown to undergo adult neurogenesis.[28] AHPCs can self-assemble and maintain their proliferative capacity to generate three dimensional (3D) cellular aggregates, neurospheroids, when cultured in the absence of extracellular matrix proteins. These AHPC neurospheroids are preferred models of studying the cellular effects of the neurotransmitters on NSC behavior as the 3D structure of the neurospheroids provide the cells with a compact microenvironment likely resulting in greater cell–cell communication and interactions compared to traditional two-dimensional (2D) cell culture methods.

As shown in Fig. 1, the AHPC neurospheroids are cultured in one chamber (*Chamber-2*) separated by a diffusion barrier from another chamber (*Chamber-1*) containing neurotransmitters. The diffusion barrier can be filled with PEG gel through Inlet-1 and Inlet-2, thereby modulating its permeability for neurotransmitters. PEG gel has been widely used for different applications such as tissue engineering,[29–31] fluorescent detection,[32] and diffusion barriers.[33–35] Herein, PEG gel is integrated within diffusion barrier *for the first time* to modulate the diffusion of neurotransmitters on chip.

2. Materials and methods

2.1 Chemicals and materials

Positive photoresist AZ 40XT and AZ 326 MIF developer were purchased from MicroChemicals (Germany). Polydimethylsiloxane (PDMS) was purchased from Dow Corning (Midland, WI, USA). Poly(ethylene glycol) (PEG, MW 2000 Da and 20 000 Da), Poly(ethylene glycol)diacrylate (PEGDA, molecular weight (MW) 700 Da), and 2-hydroxy-1-[4-(2-hydroxyethoxy)phenyl]-2-methylpropan-1-one (Irgacure 2959) were purchased from Sigma (St Louis, MO, USA). Fluorescent dye fluorescein sodium salt (FSS) was purchased from Sigma (St Louis, MO, USA).

Adult rat hippocampal progenitor cells (AHPCs) were generously gifted by Dr. F. H. Gage, Salk Institute, La Jolla, CA. Poly-L-ornithine was purchased from Sigma-Aldrich, St. Louis, MO. Laminin was purchased from Cultrex by Trevigen, Gaithersburg, MD. Maintenance media (MM) composed of Dulbecco's modified Eagle's medium/Ham's F-12 (DMEM/F-12, 1 : 1) was purchased from Omega Scientific, Tarzana, CA. GlutaMAX was purchased from Thermo Fisher Scientific, Waltham, MA. N2 supplement was purchased from Gibco by Thermo Fisher Scientific, Waltham, MA. Penicillin/streptomycin was purchased from Gibco by Thermo Fisher Scientific, Waltham, MA. Basic fibroblast growth factor (bFGF) was purchased from Promega Corporation, Madison, WI. Uncoated tissue-culture polystyrene (TCPS) culture-ware was purchased from Thermo Fisher Scientific, Waltham, MA. Propidium iodide (PI) was purchased from Thermo Fisher Scientific, Waltham, MA. Dopamine hydrochloride (DA) and serotonin hydrochloride (serotonin) were purchased from Sigma-Aldrich, St. Louis, MO. *Escherichia coli* K-12 strains were cultured using standard protocols. *E. coli* was also transformed with a recombinant plasmid expressing red fluorescent protein (RFP) to enable visualization by fluorescence microscopy.

2.2 Chip description, modeling and fabrication

Description and operation of the chip. The chip is schematically illustrated in Fig. 1A, which is composed of two adjacent chambers separated by systematically

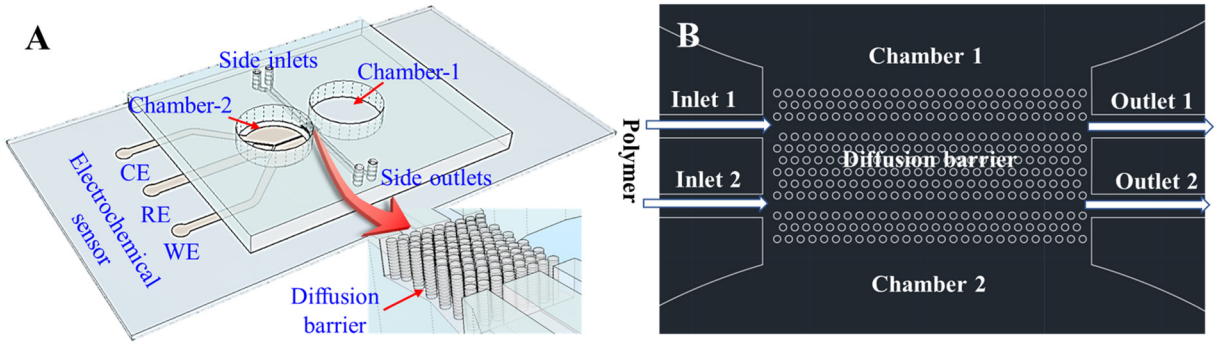

Fig. 1 (A) Schematic illustration of the chip consisting of two adjacent chambers separated by a diffusion barrier; a three-electrode electrochemical sensor is integrated inside *Chamber-2*; (B) close-up of the diffusion barrier region between *Chamber-1* and *Chamber-2*. PEG gel is injected into the gaps among the micropillars in the region of the diffusion barrier.

misaligned micropillars as a diffusion barrier. One chamber (*Chamber-1*) acts as a reservoir for neurotransmitter solutions, and the other (*Chamber-2*) is used for culturing neurospheroids. The diffusion barrier between the two chambers allows neurotransmitters' solution to diffuse into an adjacent chamber and react with the neurospheroids, which are used as an *in vitro* brain model. A close-up of the diffusion barrier is illustrated in Fig. 1B. For this design, there are 12 rows of micropillars, the adjacent rows of the micropillars are systematically misaligned, reducing the effective gaps among them, thereby increasing the fluidic resistance and slowing down the diffusion rate of the solutions of neurotransmitters from one chamber to the other. The gap between the micropillar rows is 20 μm, and the gap between adjacent micropillars within an individual row is 50 μm. To further tune the permeability of the barrier, curable PEG prepolymer was injected into the barrier region through two channels with Inlet-1/Outlet-1 and Inlet-2/Outlet-2 to fill the spacing/gaps among the micropillars as shown in Fig. 1B, forming a permeable hydrogel barrier with micro-nanoscale pores. The major parameters to affect the permeability of the diffusion barrier are the size of the micropillars, the gap among the micropillars, the number of the micropillars, and the formula of the PEG prepolymer. In addition, a three-electrode electrochemical sensor (Fig. 1A) can be integrated inside the *Chamber-2* so that the concentrations of the neurotransmitters can be monitored.

Modeling of the permeability of the diffusion barrier. Numerical calculations were carried out to simulate the diffusion of the neurotransmitters through the barrier using the COMSOL Multiphysics software (COMSOL Inc., Los Angeles, CA, USA). For simplification, it is assumed that (1) the level of the neurotransmitter (*i.e.*, dopamine or serotonin) remains constant (*i.e.*, 20 μM) in *Chamber-1* during the entire diffusion process until the concentrations of the neurotransmitters become equalized in *Chamber-1* and *Chamber-2*, and that (2) diffusion coefficients of the neurotransmitters in media and PEG gel are in a range of 1.0×10^{-9} to1.5×10^{-8} m^2 s^{-1} and 7.5×10^{-11} to 5.0×10^{-9} m^2 s^{-1},[33,34] respectively.

Fabrication of the chip. (1) Fabrication of the electrochemical sensors: the three-electrode electrochemical sensor (Fig. 1A) was fabricated on a glass coverslip using a lift-off process.[36] Briefly, a positive photoresist was patterned using optical lithography on the coverslip as a mold, followed by evaporating a layer of ~100 nm Au using ~10 nm Ti as an adhesion layer. Then the photoresist was removed by acetone and rinsed by deionized (DI) water several times.

(2) Polydimethylsiloxane (PDMS) fluidic layer was fabricated using a soft lithography process. Briefly, a mold was first fabricated from photoresist AZ40XT. Then PDMS was poured on the mold followed by 1 hour degassing and 2 hour curing at 75 °C. Thereafter, the PDMS microfluidic layer was peeled off from the mold, followed by the formation of the chambers by punching through the PDMS layer using a biopsy punch.

Finally, one type of chip, without an electrochemical sensor in *Chamber-2*, was formed by bonding the PDMS microfluidic layer to the coverslip after oxygen plasma treatment. The other type of chip, with an electrochemical sensor in *Chamber-2*, was formed by bonding the PDMS microfluidic layer to the coverslip with fabricated electrochemical sensor after oxygen plasma treatment.

Integrating the PEG hydrogel diffusion barrier to chip. Different formulas of PEG prepolymer solutions have been prepared to test the diffusion rate of the hydrogels, including 10%, 20% (w/v) of 2 k PEG, and 5%, 10%, 20%(w/v) of 20 k PEG. In addition, 5% (v/v) PEGDA and 1% (w/v) Irgacure 2959 have also been mixed into the PEG prepolymer solutions.[33] The PEG prepolymer solution was injected into the micropillar barrier region through designated channels with Inlet-1/Outlet-1 and Inlet-2/Outlet-2 that were directly connected to the barrier region (Fig. 1B) using syringe pumps (Harvard Apparatus, Inc.). Because of the micropillar barrier, the majority of the prepolymer solutions were trapped in the barrier region while a small amount of solution spread into adjacent chambers. The PEG prepolymer solutions were then converted to permeable hydrogels by a 730 second ultraviolet (UV) light (6 mW cm^{-2}) exposure. The excess hydrogel in both chambers was removed using a tweezer. Finally, the chip was immersed in phosphate buffered solution (PBS) for 2 days to remove unpolymerized PEG prepolymer. Note that after UV exposure, different

formulas of the PEG prepolymers result in permeable hydrogels with different mechanical properties, density, viscosity, pore size.[33] An optimal formula of the PEG prepolymer can be identified for constructing the diffusion barrier in the chip by experiments.

2.3 Neurospheroid cultures

AHPC neurospheroids were generated as previously described.[37] Briefly, AHPCs were cultured in uncoated T25 culture flasks using complete AHPC culture maintenance media (MM) with DMEM/F-12, supplemented with 2.5 mM GlutaMAX, 1 × N2 supplement, 1 × penicillin/streptomycin, and 20 ng mL^{-1} bFGF. This resulted in self-assembly of AHPCs generating neurospheroids that continued to proliferate. Neurospheroids were collected from the T25 flask and transferred to a 15 mL conical tube where the neurospheroids were allowed to settle. Once a pellet formed at the bottom of the tube, the supernatant was removed at the cells were rinsed three times with 1 mL fresh MM to remove any debris from the cell suspension. The neurospheroid pellet was resuspended in 1 mL fresh MM. 50 μL of cell suspension was seeded into *Chamber-2* of the chip with an equal volume of MM was added to *Chamber-1* to ensure equal diffusion across the pillar region. For control samples, 100 μL of cell suspension was added to 400 μL MM in wells of an uncoated 24-well plate.

Twenty-four hours after cell seeding, the drug treatment protocol began. To administer the drug treatment, the MM within the microfluidic devices and 24-well plates was replaced with differentiation media (DM; MM without bFGF) containing various concentrations of the drug treatment. For the chips, the drug treatment was added to *Chamber-1*. The DA and L-DOPA treatments were added at a concentration of 20 μM for both the chips as well as the 24-well plate. The serotonin treatment was added at concentrations of 1 or 5 μM within the chips or concentrations of 1, 5, 10, or 25 μM within the 24-well plate. Carrier control (dH_2O) was used for the non-drug treated controls. The drug treatment was replenished every day *via* half-media changes for up to 7 days-*in vitro* (DIV).

2.4 Immunocytochemistry (ICC)

All cell staining and immunocytochemical procedures were conducted on chip or within the wells of the 24-well plates. Briefly, the chamber with neurospheroids was rinsed with 0.1 M PO_4 buffer, and then fixed with 4% paraformaldehyde (PFA, Thermo Fisher Scientific) in 0.1 M PO_4 buffer for 20 minutes. Fixation was followed by three, 7 minute phosphate buffered saline (PBS) washes. The cells were incubated in blocking solution: 0.2% Triton X-100 (Thermo Fisher Scientific), 5% normal donkey serum (NDS) (Jackson ImmunoResearch), and 0.4% bovine serum albumin (BSA) (Sigma-Aldrich) in PBS at room temperature for 1.5 h. Primary antibodies Rabbit α Ki-67 (1 : 100, IgG; Abcam), and Mouse α TuJ1 (1 : 100, IgG; R&D Systems) were diluted in the blocking solution. The cells were incubated with the primary antibody solution overnight at 4 °C. After rinsing with PBS four times for eight minutes each, the microchamber or well was loaded with secondary antibody solution. To prepare the secondary antibody solution, Donkey α Rabbit Cy3 (1 : 100, IgG; Jackson ImmunoResearch), and Donkey α Mouse AF488 (1 : 100, IgG; Jackson ImmunoResearch) were diluted with the blocking solution containing 4′,6-diamidino-2-phenylindole (DAPI; diluted 1 : 1000; Invitrogen). Again, the cells were incubated with the secondary antibody solution under room temperature in the dark for 1.5 h. After rinsing with PBS four times for eight minutes each, the cells were ready for fluorescence imaging.

2.5 Propidium iodide (PI) staining and cell viability test

Propidium iodide was used to stain dead cells as an indicator of cell viability. A 1.5 μM PI solution was prepared by diluting the stock solution in culture medium, which was then loaded into the culture chamber, followed by incubation for 20 min at 37 °C in 5% CO_2. As a reagent control, another chip or well of the 24-well plate containing AHPC neurospheroids was loaded with 70% ethanol for 5 min to intentionally kill all the cells prior to adding the PI solution. After PI incubation, the neurospheroids were rinsed with 0.1 M PO_4 buffer and then fixed with 4% PFA for 20 minutes. After rinsing with PBS three times for seven minutes each, the cells were incubated with DAPI (1 : 1000) diluted in blocking solution for 60 min at room temperature in the dark, followed by four, eight-minute rinses with PBS.

2.6 Evaluation of *E. coli* diffusion through the diffusion barriers in chips

E. coli solution was loaded into *Chamber-1* of the chips with different types of diffusion barriers using a pipette. Then the chips were kept in the ambient conditions at room temperature. The fluorescence images were taken periodically up to 15 days.

2.7 Imaging

Phase contrast images of AHPC neurospheroids were taken with a Nikon Diaphot inverted phase contrast microscope (Nikon Corp.) equipped with a Q Imaging Retiga 2000R (Q Imaging) digital camera daily so that cell growth and neurospheroid development could be monitored. Corresponding fluorescence images following immunocytochemistry and PI staining were taken using a Leica DMI4000 B (Leica Microsystems) inverted microscope equipped with standard epifluorescence illumination and a Leica DFC310 FX digital camera. A 20× objective was used to obtain images for quantitative data analysis.

2.8 Data acquisition and statistical analysis

ImageJ software (**https://imagej.net/ij/index.html**) was used to analyze and quantify the images of neurospheroids. Ki-67

and TuJ1 immunopositive cells were counted using the Cell Counter tool in ImageJ and the % of Ki-67 or TuJ1 immunoreactive cells was determined as the number of Ki-67 labeled nuclei or TuJ1 labeled cytoskeleton over the total DAPI-labeled nuclei. All means are reported with standard error of the mean (mean ± SEM). Graph Pad Prism 9 (Graph Pad Software, Inc. San Diego, CA) was used for statistical analysis and graph-making. Means were compared using ordinary one-way ANOVA. Statistical significance determined using Tukey's multiple comparison test, with alpha = 0.05.

3. Results and discussion

3.1 Calculation of neurotransmitter diffusion through the diffusion barrier

The results of modeling neurotransmitter diffusion, as shown in Fig. 2, demonstrated that the different permeability of diffusion barrier results in different time durations for the establishment of neurotransmitter concentration gradients within the chambers on the chip. Diffusion coefficients of the neurotransmitters, spanning from 1.0×10^{-9} to 1.5×10^{-8} $m^2\ s^{-1}$ in media and from 7.5×10^{-11} to 5.0×10^{-9} $m^2\ s^{-1}$ in PEG gel, respectively, have been used for the numerical calculations.[33,34] The diffusion direction of the neurotransmitter inside a chip is illustrated in Fig. 2A. Two types of chips have been modeled. One type of chip (Chip 1) had only misaligned micropillars as the diffusion barrier (Fig. 2B). In another type (Chip 2), the gaps among micropillars were filled with PEG gel (Fig. 2C). The representative concentration profiles of the neurotransmitter after a certain different diffusion time for Chip 1 and Chip 2 are shown in Fig. 2B and C, respectively. The ratios of the neurotransmitter's concentrations (C2/C1) in *Chamber-2* to *Chamber-1* for Chip 1 and Chip 2 are plotted in Fig. 2D and E, respectively. C2/C1 = 1 denotes the concentrations in both chambers become equalized, while C2/C1 = 0 denotes no transmitter inside *Chamber-2*. For Chip 1, the concentrations of the neurotransmitter in both

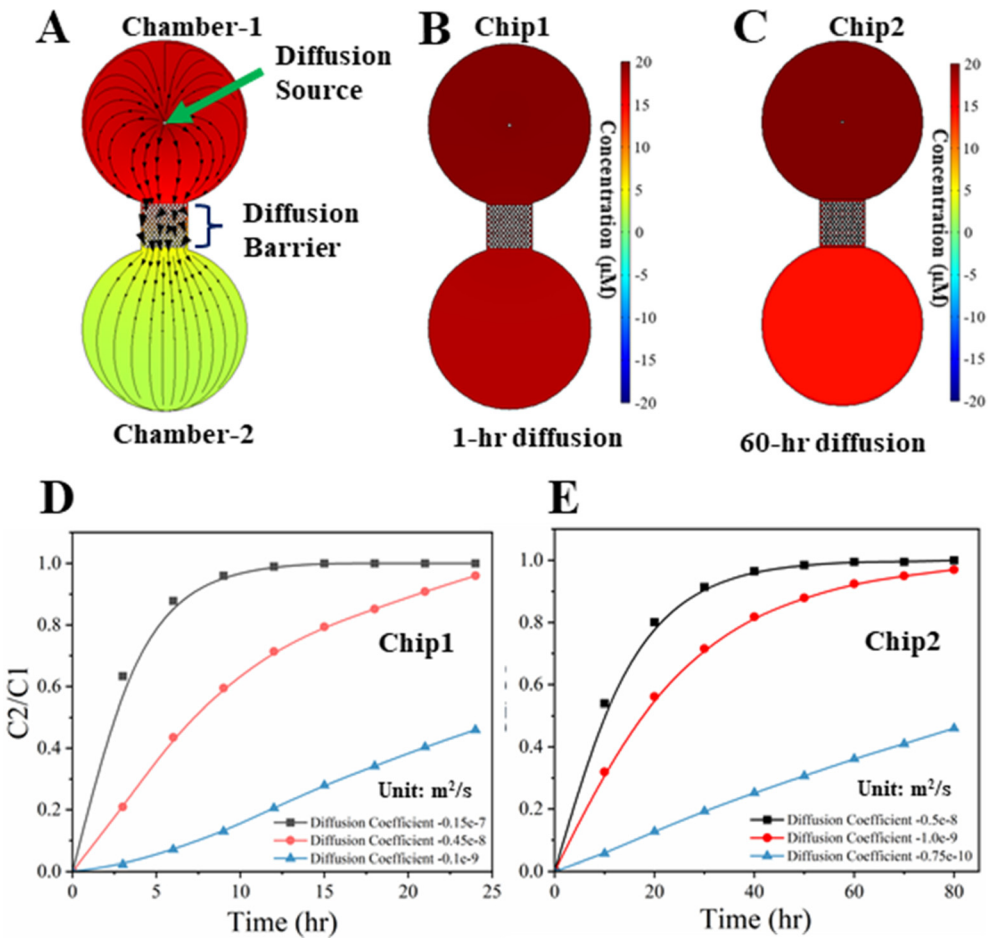

Fig. 2 Numerical calculation of the neurotransmitter (20 μM dopamine or serotonin) diffusion through the diffusion barrier: (A) diffusion direction of the neurotransmitter from *Chamber-1* to *Chamber-2*; (B) the concentration profile of the neurotransmitter in both chambers after 1 h diffusion of Chip 1. No gels are filled with the spacing/gaps among the micropillars; (C) the concentration profile of the neurotransmitter in both chambers after 60 h diffusion of Chip 2. PEG gels are injected into the spacing/gaps among the micropillars. (D) The concentration ratio (C2/C1) of the neurotransmitter in *Chamber-2* over *Chamber-1* for Chip 1 for different diffusion coefficients of the neurotransmitters in media. (E) The concentration ratio (C2/C1) of the neurotransmitter in *Chamber-2* over *Chamber-1* for Chip 1 for different diffusion coefficients of the neurotransmitters in PEG gel.

chambers can be equalized in ~10 h if the diffusion coefficients of the neurotransmitters in media is 1.5×10^{-8} m^2 s^{-1}, shown in Fig. 2D. In contrast, for Chip 2, the concentrations of the neurotransmitter in both chambers still have clear difference even after 60 h diffusion if the diffusion coefficients of the neurotransmitters in PEG gel is 1.0×10^{-9} m^2 s^{-1} (Fig. 2E). It should be noted that the diffusion coefficients for neurotransmitters in the media of different components and the PEG gels of different compositions are different, and these calculated results are based on some of

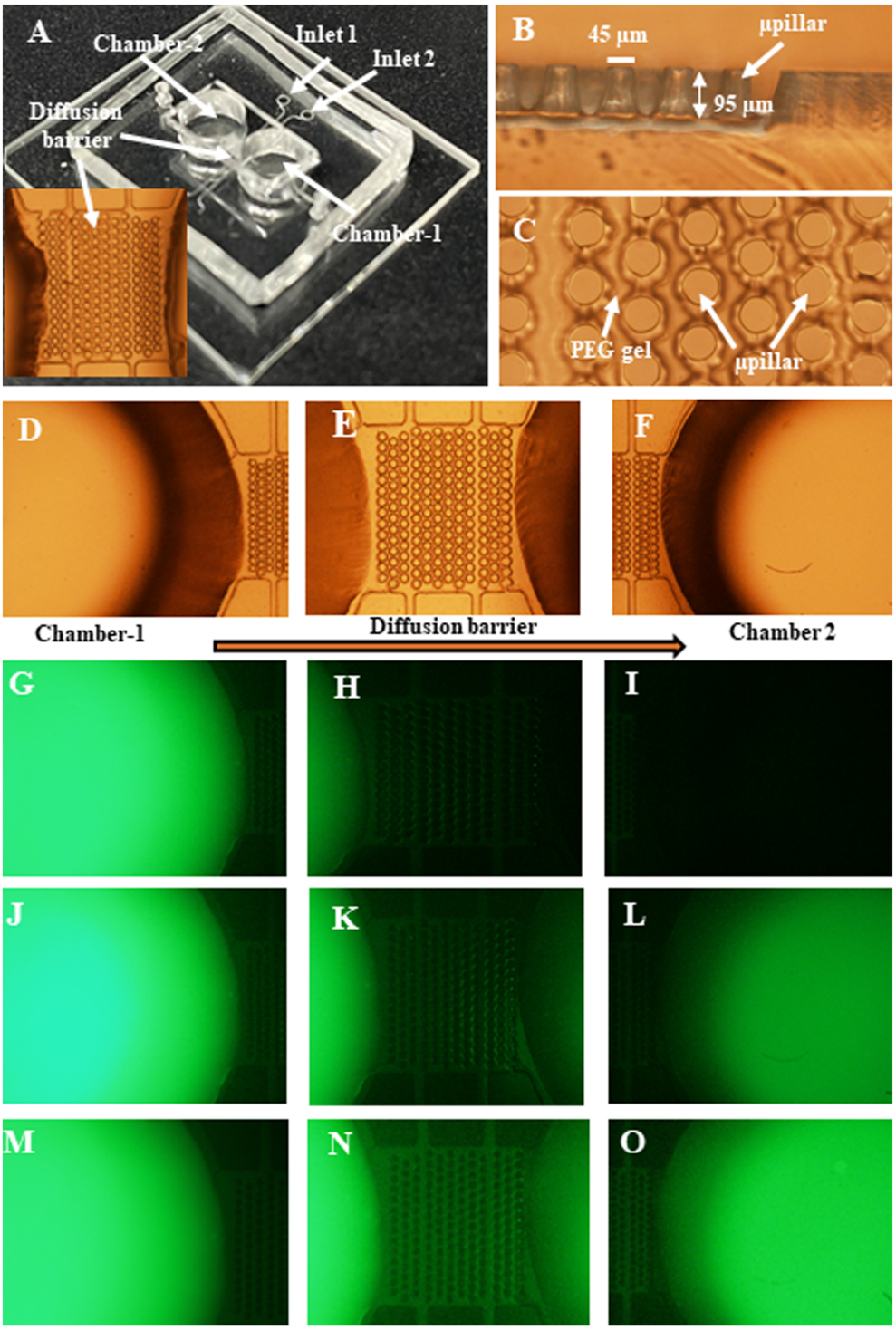

Fig. 3 Fabricated chip and its diffusion barrier. (A) Photo of a fabricated chip; (B) cross-sectional view and (C) top-side view (C) of the micropillars and PEG gel inside the diffusion barrier; (D–F) optical micrographs showing the regions of *Chamber-1*, diffusion barrier, and *Chamber-2*; fluorescent images showing the fluorescent dye FSS diffuses from *Chamber-1* to *Chamber-2* through the different barriers for Chip 1 with a diffusion time of (G–I) 0 min; (J–L) 5 h; (M–O) 24 h.

their reported values.[33–35] Hence, the modeling results are only *qualitative*. Despite this, the diffusion times are clearly highly related to the diffusion coefficients of the neurotransmitters in media and PEG gel. The smaller the diffusion coefficients, the longer diffusion time for the neurotransmitters reaching the same C2/C1. To accurately evaluate the diffusion process of the neurotransmitters, their diffusion coefficients need to be determined experimentally.

3.2 Fabricated chip and evaluation of the diffusion barrier

A photo of a fabricated chip is shown in Fig. 3A. An optical micrograph of the cross-sectional view of the micropillars in the diffusion barrier region is shown in Fig. 3B. The top-side view of the micropillars in the diffusion barrier region filled with the PEG gel is shown in Fig. 3C. Typical diameter and height of the micropillars are 45 μm and 95 μm, respectively. The gap between adjacent micropillars in the same row is 50 μm.

Diffusion of a solution (a fluorescent dye or green food dye for visibility) through the barrier has been demonstrated from *Chamber-1* to *Chamber-2*. Some representative fluorescent images of FSS diffusion from *Chamber-1* to *Chamber-2* through the diffusion barrier on Chip 1 at several time points are shown in Fig. 3G–O. As shown, the fluorescent intensity in both chambers will gradually approach to the same level with increased diffusion time from 0 to 24 h. In addition, as two representative results for green food dye, experiments have found that it takes ~1 h for the dye to diffuse from *Chamber-1* to *Chamber-2* for Chip 1 as shown in Fig. S1A and B.† Namely, the concentration of the food dye in *Chamber-2* can be almost equal to that in *Chamber-1* over 1 h. In contrast, it takes much longer time (*i.e.*, up to tens of days) for the dye to diffuse from *Chamber-1* to *Chamber-2* for Chip 2, depending on the molecular weight of PEG prepolymer. Representative photos before and after food dye diffusion from *Chamber-1* to *Chamber-2* are given in Fig. S1C and D.† For Chip 2, the concentrations of food dye *still* cannot be *really* equalized in both chambers over 10 days because of the PEG gel-based diffusion barrier. Note that during the experiments, 5% 20 K PEG was identified as one optimal formula for our experiments. Hence, unless otherwise specifically mentioned, the barrier of the Chip 2 in the experiments was formed by injecting and curing 5% 20 k PEG in the diffusion barrier. As shown in the following sections, this type of diffusion barrier allows the neurotransmitters to diffuse from *Chamber-1* to *Chamber-2* (Fig. 4). Meanwhile it can prevent the *E. coli* from passing through it (Fig. 8). Note that the diffusion barrier will be under further modifications to mimic the blood brain barrier (BBB) by culturing cortical astrocytes and endothelial cells inside spacing/gaps among the micropillars.[38–41]

3.3 Diffusion of neurotransmitters measurement

We measured the concentrations of dopamine and serotonin diffused through the diffusion barrier using the integrated electrochemical sensors. Two types of samples were prepared. One type of sample (Sample-1) was prepared by mixing deionized (DI) water and neurotransmitters (dopamine or serotonin). Another type of sample (Sample-2) was prepared by mixing neurotransmitters in standard AHPC cell culture differentiation media (DM). As technical demonstrations, the concentrations of neurotransmitters were 0.5 mM for each sample type. Experiments were carried out *either* in room temperature conditions *or* in an incubation chamber (temperature: 37.0 °C, CO_2: 5.0%).

Measurements of neurotransmitters were taken using a three-electrodes electrochemical sensor since the neurotransmitters (dopamine or serotonin) are electroactive chemicals that are oxidized in the presence of electric potential.[42] Specifically, cyclic voltammetry was used as an electrochemical detection method. As shown in Fig. 4A, *Chamber-1* was filled neurotransmitter with the sample while *Chamber-2* was filled with only solution without neurotransmitters at room temperature. Then cyclic voltammogram (CV) was recorded every hour using a potentiostat (Digi-Ivy, Inc.). A representative CV of dopamine and serotonin over time is shown in Fig. 4B and C, respectively. It has been found that dopamine and serotonin has an oxidation potential of ~0.2 volts and 0.3 volts, respectively, consistent with those reported previously.[42,43] When Sample-1 was measured in Chip 1 at room temperature, the peak current increases over time from ~2.0 μA after 3 hour diffusion to 6.0 μA after 15 hour diffusion, verifying that the serotonin was able to diffuse through the diffusion barrier from *Chamber-1* to *Chamber-2* (Fig. 4D). Similar experiments were carried out for dopamine (Fig. 4D). For dopamine and serotonin, the peak currents reached a maximum of ~6 μA after ~10 h diffusion and 5 μA after ~24 hour diffusion, respectively, indicating their concentrations approach saturation in *Chamber-2*. In contrast, it took approximately 60 to 70 hours for the concentrations of dopamine or serotonin to approach saturation in *Chamber-2* when Sample-1 was measured in Chip 2 (Fig. 4E). Clearly, a longer time was required for Chip 2 than Chip 1 to establish saturated concentrations for dopamine or serotonin in *Chamber-2*. Again the barrier of Chip 2 in these experiments was formed by injecting and curing 5% 20 k PEG in the diffusion barrier. The calibration curves of the peak currents *vs.* concentrations of serotonin and dopamine in DI water (Fig. 4F) were measured using the electrochemical sensors with good linearity, consistent with previously reported work.[42] Based on the calibration curves, the calculated concentrations of serotonin and dopamine *vs.* diffusion time using Chip 1 is shown in Fig. 4G. Clearly, their concentrations in *Chamber-1* and *Chamber-2* gradually approached to ~0.25 mM, indicating the neurotransmitters passed the diffusion barrier. As a result, the concentrations in both chambers essentially become equalized (~0.25 mM). Similar results have been observed in Fig. 4H for Chip 2.

For dopamine and serotonin in Sample-2, the peak currents reached maximum after ~24 hour diffusion in Chip 1, indicating their concentrations approached saturation in

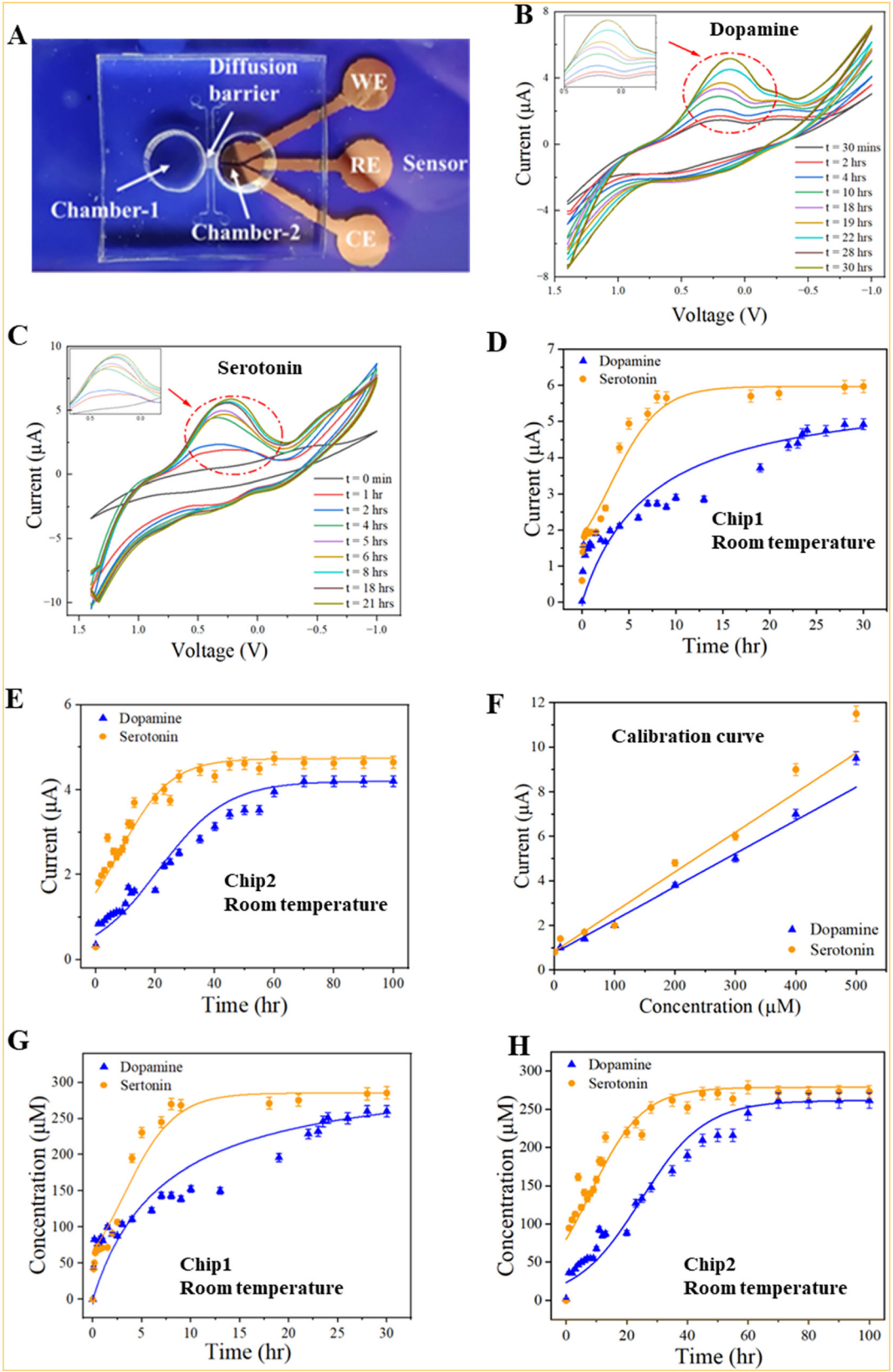

Fig. 4 (A) Photo of a chip with an integrated three-electrode electrochemical sensor; (B and C) representative measured CV curves of dopamine and serotonin at different time points in *Chamber-2*; (D) measured current *vs.* diffusion time for dopamine and serotonin in DI water in *Chamber-2* using *Chip 1* at room temperature; (E) measured current *vs.* diffusion time for dopamine and serotonin in DI water in *Chamber-2* using *Chip 2* at room temperature; (F) measured currents of dopamine and serotonin at different concentrations in DI water as a calibration curve; (G) calculated concentrations of dopamine and serotonin in *Chamber-2* using Chip 1 at different time points; (H) calculated concentrations of dopamine and serotonin in *Chamber-2* using Chip 2 at different time points. Error bars were obtained by calculating standard deviation values.

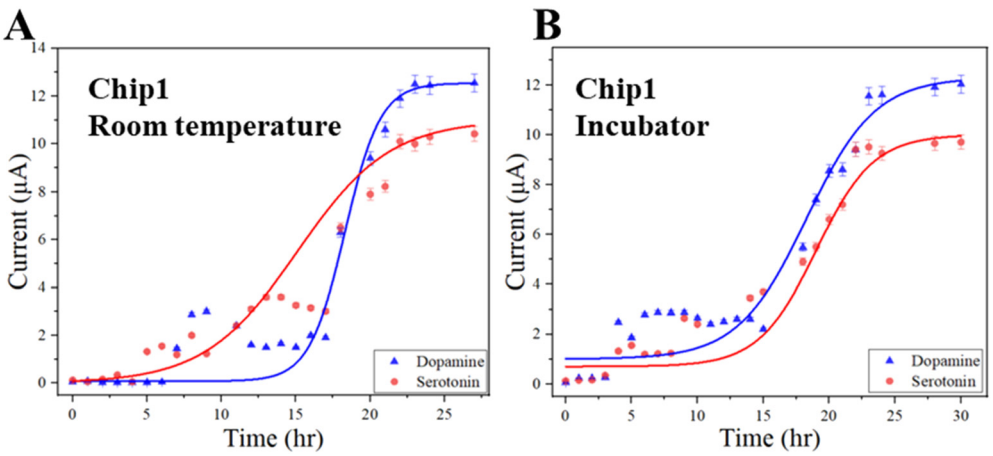

Fig. 5 Measured current *vs.* diffusion time for (A) dopamine and serotonin in differentiation media (DM) in *Chamber-2* using *Chip 1* at room temperature; measured current *vs.* diffusion time for (B) dopamine and serotonin in DM in *Chamber-2* using *Chip 1* in an incubator. Error bars were obtained by calculating standard deviation values.

Chamber-2 (Fig. 5A). But the measured currents did not follow the same patterns as those of Sample-1 as shown in Fig. 4D and E. This was likely possible due to the biofouling of the biomolecules inside the differentiation media on the top surface of the sensing electrode. It took a longer time for the dopamine or serotonin to reach the sensor surface, resulting in the delayed signals. Measurements were also carried out in an incubation chamber to observe the diffusion of neurotransmitters under cell culture environmental conditions. Similar diffusion patterns were observed in these experiments to those at room temperature (Fig. 5B). It took approximately 24 hours for dopamine or serotonin to approach saturation in *Chamber-2*.

3.4 Effects of neurotransmitters on neurospheroids

A preliminary test of each neurotransmitter concentration was evaluated within a 24-well plate under a concentration gradient to select the ideal concentrations for use within the chips. The results showed the 1 μM and 5 μM serotonin treatments had the lowest level of PI-labeling of the tested conditions, while the 25 μM treatment resulted in an increase in the number of dead cells based on the PI-labeling (not shown). Similar trends were seen for Ki-67 and TuJ1 expression with the 1 μM and 5 μM having the most positive effect on their expression level while 25 μM treatment resulted in a notable decrease in expression (not shown). For the dopamine tests, the 10 μM treatment had little effect on cell viability while the 50 μM and 100 μM treatments resulted in a high level of cell death within the cultures. The percentage of Ki-67 expression and TuJ1 expression also did not appear to change following 10 μM treatment compared to the control with the level of expression appearing to decrease for the 50 μM and 100 μM treatments, likely due to the high level of PI staining seen for these groups (not shown). As such, within the chips, the serotonin treated samples were treated at concentrations of 1 μM or 5 μM. For the dopamine treated samples, a concentration of 20 μM was selected as this fell within the effective concentration range to modulate cellular processes without being cytotoxic.

Cell viability. To determine the effect of the neurotransmitters on cell viability *inside the chips*, the neurospheroids were treated with serotonin or dopamine then a propidium iodide (PI) cell viability assay was performed at 3 and 7 DIV to evaluate the percentage of dead cells within the neurospheroid cultures. As seen in the representative fluorescent images of the PI staining at the 7 DIV timepoint shown in Fig. 6A–P, the percentage of PI labeled cells did not appear to change significantly with the increase in serotonin concentration. At the 3 DIV timepoint, there was a slight, but significant, decrease in the percentage of PI-labeled cells for the 5 μM treated samples compared to the 1 μM treatment; however, neither serotonin treated group showed significant difference from the control group (Fig. 6Q). When evaluating the percentage of PI-labeled cells at the 7 DIV timepoint, no significant difference was seen between any of the treatment groups with or without serotonin treatment (Fig. 6Q). Overall, the neurospheroids remained highly viable following serotonin treatment showing 98.7–98% viability. Similarly, the 20 μM DA treatment also did not significantly affect cell viability within the neurospheroid within the microfluidic devices (Fig. S2A–P†). The DA treated cells showed a viability ranging between 95.1–97.7% (Fig. S2Q†).

Cell viability trials were also performed on neurospheroids cultured within 24-well plates at the same concentrations used within the chips to act as a cell culture platform control. The results of the cell viability analysis within the 24-well plates showed the cells retained high viability ranging between 97.1–98.3% following serotonin treatment and 96–97.7% following dopamine treatment (not shown). These results highlight that normal growth patterns were observed for the neurospheroids cultured in the chips given that a similar cell viability was seen for all treatments within both culture platforms.

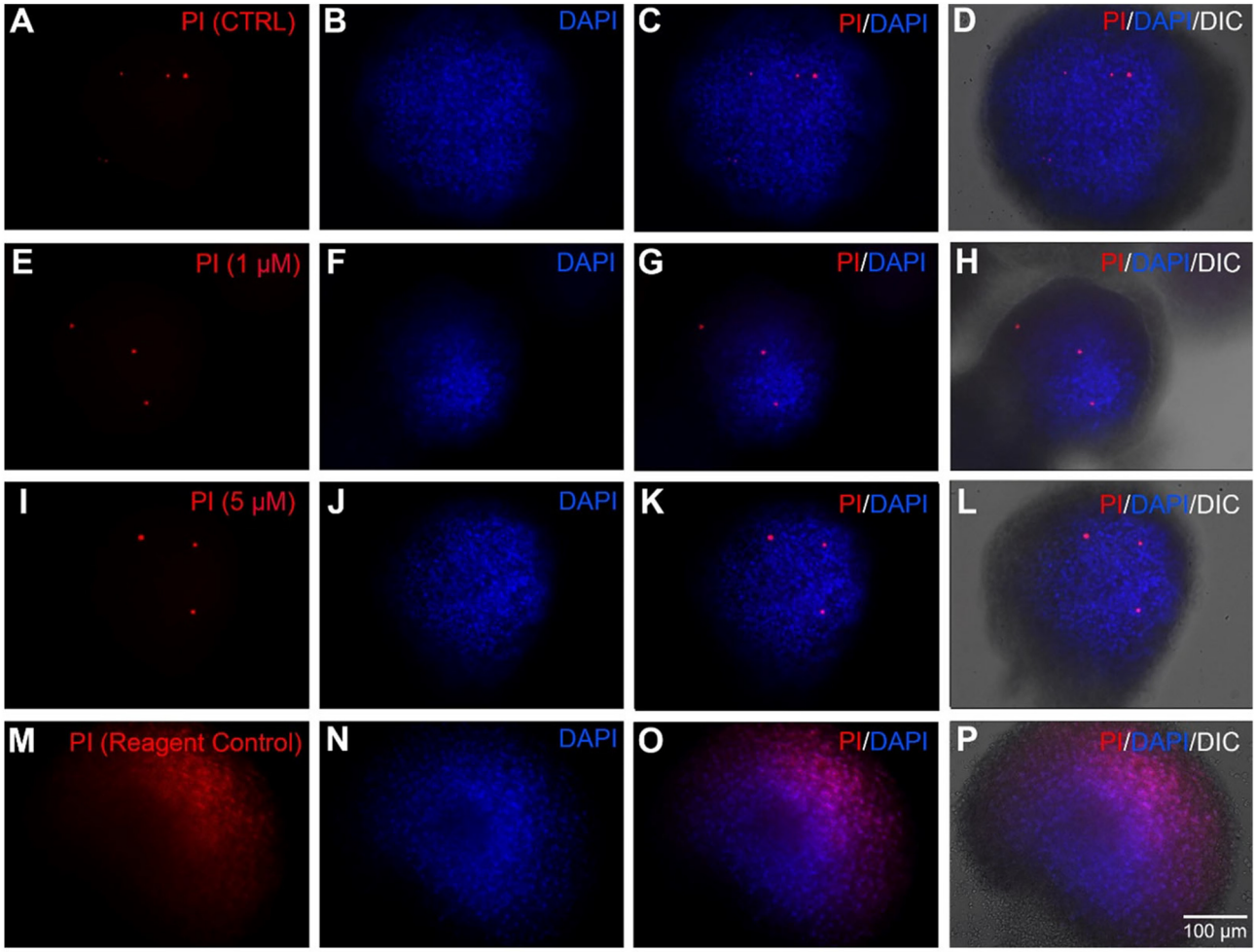

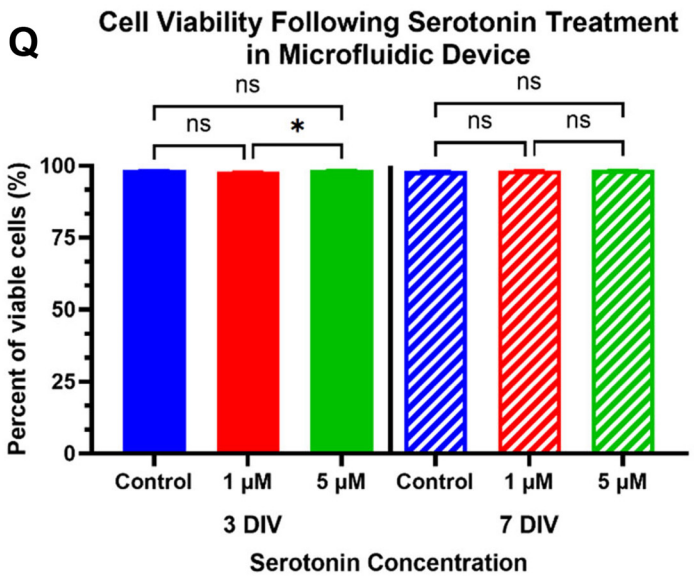

Fig. 6 Viability of AHPC neurospheroids under serotonin treatment in microchips. A–P: Fluorescence images of AHPC neurospheroids at 7 DIV following serotonin treatment in microfluidic devices. Propidium iodide staining of dead cells (PI, red; A, C, D, E, G, H, I, K, L, M, O, and P) and cell nuclei stained with DAPI (blue; B, C, D, F, G, H, J, K, L, N, O, and P). Cells intentionally killed with 70% ethanol acted as a positive reagent control for PI staining (M–P). Scale bar = 100 μm. Q: Quantitative analysis of AHPC cell viability following drug treatment within microfluidic devices at 3 and 7 DIV. There was a slight, yet significant decrease in the percentage of PI-labeled cells following 5 μM treatment compared to 1 μM treatment at 3 DIV; however, no significant difference was seen between any of the culture conditions at 7 DIV. Bars represent the mean percentage of PI-labeled cells, and the error bars represent the standard error of the mean. *N* = 3 independent experiments, 24–29 images were quantified for each treatment condition.

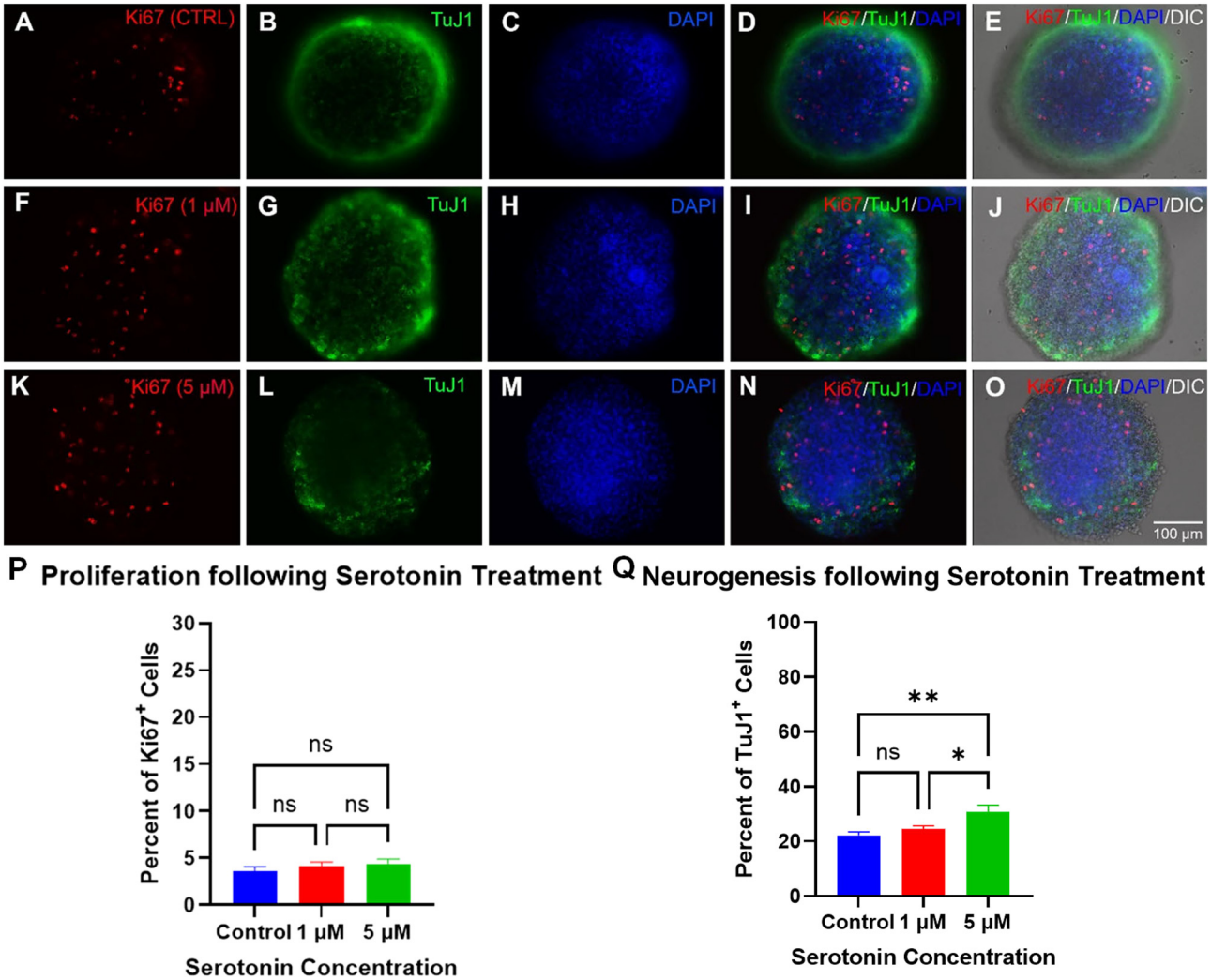

Fig. 7 Proliferation and differentiation of AHPC neurospheroids under serotonin treatment in microchips. A–P: Fluorescence images of AHPC neurospheroids at 7 DIV following serotonin treatment in microfluidic devices. Cells were immunolabeled with cell proliferation marker, Ki-67 (red; A, D, E, F, I, J, K, N, and O), immature neuron marker, TuJ1, (green; B, D, E, G, I, J, L, N, and O), and cell nuclei stained with DAPI (blue; C, D, E, H, I, J, M, N, and O). Scale bar = 100 μm. P and Q: Quantitative analysis of AHPC cell proliferation and differentiation following drug treatment within microfluidic devices at 7 DIV. P: There was no significant difference in the percent of Ki-67-labled cells following serotonin treatment compared to the control or between serotonin concentrations. Q: A significant increase in neurogenesis (TuJ1-labeled cells) was observed following 5 μM serotonin treatment compared to the control and 1 μM. The 1 μM treatment group was not significantly different from the control group. Bars represent the mean percentage of PI-labeled cells, and the error bars represent the standard error of the mean. *N* = 3 independent experiments, 30 images were quantified for each treatment condition.

Proliferation analysis. A proliferation analysis was performed on the neurotransmitter treated samples at the 7 DIV timepoint using Ki-67 as a marker for proliferating cell *inside the chips*. Fluorescent images show that following serotonin treatment, there did not appear to be a change in the level of Ki-67 expression with an increase in serotonin concentration within the microfluidic devices (Fig. 7A–O). The percentage of the Ki-67 positive cells ranged from 3.6–4.4% between the treatment conditions with a slight, but non-significant, increase in expression with increased serotonin concentration (Fig. 7P). Similar results were seen following dopamine treatment (Fig. S3A–O†). Again, there was a slight, but non-significant, increase in the Ki-67 expression following dopamine treatment in the percentage of Ki-67 expressing cells increasing from 3.9% to 5.7% (Fig. S3P†).

The 24-well plate cell culture controls showed similar results to those seen within the chips. The percentage of Ki-67 expressing cells did not differ between the culture platforms within the treatment groups. The percentage of Ki-67 expressing cells within the 24-well plate for the serotonin treated samples ranged from 4.3–5.6% while the expression level for the dopamine-treated samples ranged from 3.8–6.8% (not shown). This, again, suggested that the neurospheroid proliferation behavior was not being affected as a result of differences in the cell culture platforms.

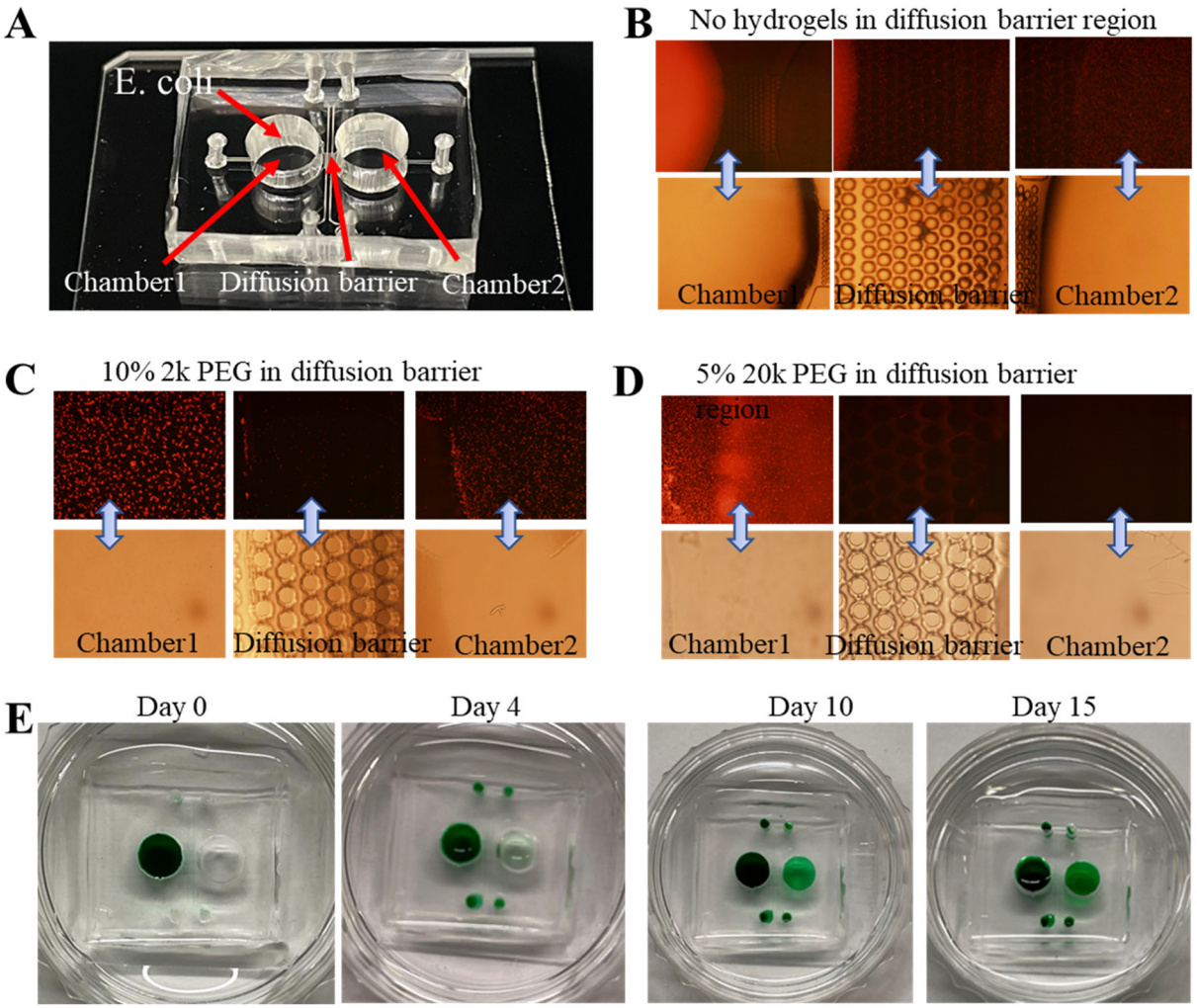

Fig. 8 (A) Photo of a chip for evaluating diffusion of *E. coli* and food dye through the diffusion barrier; (B) fluorescent images (top row) and the optical images (bottom row) of *Chamber-1*, diffusion barrier and *Chamber-2* for Chip 1; (C) fluorescent images (top row) and the optical images (bottom row) of *Chamber-1*, diffusion barrier and *Chamber-2* for Chip 2 with 10% 2 K PEG in the diffusion barrier; (D) fluorescent images (top row) and the optical images (bottom row) of *Chamber-1*, diffusion barrier and *Chamber-2* for Chip 2 with 5% 20 K PEG in the diffusion barrier; (E) photos showing the blue food dye diffuses from *Chamber-1* to *Chamber-2* through the diffusion barrier for Chip 2 with 5% 20 K PEG in the diffusion barrier.

Neurogenesis analysis. To determine the effect of neurotransmitter exposure on neurogenesis *inside the chips*, TuJ1 was used as a marker for neuronal differentiation. TuJ1 labels immature neurons, and as such is an effective indicator for the presence of emerging neurons within the neurospheroids. After serotonin treatment there appeared to be an increase in the level of TuJ1 expression with increased concentration of serotonin (Fig. 7A–O). The 5 μM treatment was shown to significantly increase the percentage of TuJ1 positive cells compared to both the non-treated control and 1 μM treated neurospheroids, with the percent increasing to 30.8% compared to 22.2% and 24.4%, respectively (Fig. 7Q). Similarly, dopamine treatment also appeared to increase in the percentage of TuJ1 expressing cells (Fig. S2A–O†). However, while the percentage of TuJ1 positive cells increased from 13.3% to 15.8% following DA treatment, this increase was non-significant (Fig. S2Q†).

Unlike the previous analyses, there was a difference in the percentage of TuJ1 labeled cells between the 24-well plate control and those seen in the chips. While the control conditions did not show a significant difference in TuJ1 expression between the culture platforms, the dopamine treatment showed a significant increase in expression within the neurospheroids grown in the 24-well plate compared to those grown in the chips (not shown). The serotonin treatments also showed a slight increase in TuJ1 expression in the neurospheroids cultured in the 24-well plate compared to the chips, but the difference was not a significant as those seen for the dopamine. One possible explanation for this discrepancy could be due to the more turbulent fluid flow within the wells of the 24-well plate causing the neurospheroids to aggregate to single large neurospheroids within the well resulting in more cell–cell interactions between the cells. This increase in cell–cell interactions could

increase cell signaling pathways within the neurospheroids to increase TuJ1 expression.

3.5 Tunable permeability of the diffusion barrier for *E. coli* and neurotransmitters

The chip-based approach holds the potential to reveal new mechanistic insights into gut microbiome–brain communication.[44,45] *Escherichia coli* is a common bacterium in the mammalian gastrointestinal tract, and part of the normal gut microbiota in humans.[46] The contribution of specific bacterial species capable of producing neurotransmitters can be further tested using bacteria that naturally produce specific neurotransmitters, or are so enabled by genetic engineering.[47–50]

To fully develop the potential of this chip-based approach for *in vitro* studies of the interactions of the brain model (*i.e.*, neurospheroids) with the neurotransmitters released by *E. coli*, the diffusion barrier inside the chip needs to be optimized so that *E. coli* cannot pass the barrier while the neurotransmitters can. Therefore, chips with *several different diffusion barriers* were tested. Three representative chips are shown in Fig. 8B–D. Non-pathogenic strains of *E. coli* K-12 were genetically tagged with red fluorescent protein (RFP) and serially diluted by a factor of 10. 100 μL 10^{-2} (1 : 100 dilution) and 10^{-3} (1 : 1000 dilution) *E. coli* suspensions are transferred into *Chamber-1* and 100 μL DI water is loaded to *Chamber-2* of the chips. The chips have six different types of diffusion barriers, including one without PEG gel and five injected with different PEG prepolymer formulas. Both optical images and fluorescent images of the *Chamber-1* region, diffusion-barrier region and *Chamber-2* region are taken every 24 hours by a fluorescent microscope.

As shown in Fig. 8A, *E. coli*, typically with 1–2 μm in length, is cultured in *Chamber-1*. For Chip 1, it was observed that *E. coli* can easily go through the diffusion barrier and arrive at *Chamber-2* based on the fluorescence images in Fig. 8B. For Chip 2, in Fig. 8C, the diffusion barrier inside the chip included cured 10% 2 k PEG, it has been observed that *E. coli* can still pass the barrier to reach *Chamber-2*. By injecting and curing 5% 20 k PEG in the diffusion barrier, *E. coli* cells can be completely blocked from reaching *Chamber-2*, based on the fluorescence images in Fig. 8D.

To test if the chip used in Fig. 8C and D could still allow dopamine or serotonin to pass through the barrier, green dye (Fast Green FCF) was used as a mimic for visibility and added to *Chamber-1* instead of *E. coli*. For Chip 2 of Fig. 8C, green dye could pass through the barriers and its concentration approaches saturation within several days (*not shown*). In contrast, for Chip 2 of Fig. 8D, *E. coli* could not penetrate the diffusion barrier, the green dye could be observed in *Chamber-2* 4 days later as shown in Fig. 8E. The concentration of the dye in *Chamber-2* increased but remained lower than that in *Chamber-1* even after 2 weeks. The size of Fast Green FCF is much larger than those of dopamine and serotonin (Table S1†), suggesting dopamine and serotonin can pass the barrier of the Chip 2 of Fig. 8D as well, which is consistent with the results in Fig. 4E of Chip 2. Based on these experiments, it is clear that Chip 2 with cured 5% 20 k PEG prepolymer inside the diffusion barrier represents a near-optimal chips to allow small molecules (*i.e.*, dopamine or serotonin) to pass through but prevent microorganisms from passing through the barrier. Hence this type of chip is suitable for carrying out the experiments to study features of the gut–brain axis.[44]

4. Conclusions

A microchip with a diffusion barrier has been developed to evaluate the effects of neurotransmitters, including serotonin and dopamine, on APHC neurospheroids. With an integrated sensor in the chip, the concentrations of the neurotransmitters, diffused from one chamber to the other chamber can be monitored. In addition, the permeability of the built-in diffusion barrier in the chip can be tuned by modifying the compositions of the PEG gel. Collectively these features pave the way for *in vitro* studies of the interactions between the microbiota and brain tissue using chip-based technologies. It has been found that the AHPCs remained highly viable and capable of proliferation and neuronal differentiation after the treatments of serotonin and dopamine. Collectively, these results indicate that the AHPC neurospheroids can be used as an *in vitro* brain model for neurogenesis research. In the future, the built-in diffusion barrier can be modified by culturing cortical astrocytes and endothelial cells inside spacing/gaps among the micropillars as the *in vitro* BBB. Also, new chips with arrayed chambers interfaced with a microfluidic network can be developed for multiplexed screening of the effects of a panel of neurotransmitters on brain models while the concentrations of the neurotransmitters can be monitored *in real time*.

Conflicts of interest

There are no conflicts to declare.

Acknowledgements

We would like to thank John Swanson and Anna Garbe, who helped with the imaging and data collection. This research was funded in part by NSF Award ECCS 2024797.

References

1 A. Alvarez-Buylla and D. A. Lim, For the long run: maintaining germinal niches in the adult brain, *Neuron*, 2004, **41**(5), 683–686.
2 P. Taupin and F. H. Gage, Adult neurogenesis and neural stem cells of the central nervous system in mammals, *J. Neurosci. Res.*, 2002, **69**(6), 745–749.
3 M. Uz, *et al.*, Advances in controlling differentiation of adult stem cells for peripheral nerve regeneration, *Adv. Healthcare Mater.*, 2018, **7**(14), 1701046.

4 D. A. Berg, *et al.*, Neurotransmitter-mediated control of neurogenesis in the adult vertebrate brain, *Development*, 2013, **140**(12), 2548–2561.
5 P. S. Eriksson, *et al.*, Neurogenesis in the adult human hippocampus, *Nat. Med.*, 1998, **4**(11), 1313–1317.
6 N. S. Roy, *et al.*, In vitro neurogenesis by progenitor cells isolated from the adult human hippocampus, *Nat. Med.*, 2000, **6**(3), 271–277.
7 H. Lee and S. Thuret, Adult human hippocampal neurogenesis: controversy and evidence, *Trends Mol. Med.*, 2018, **24**(6), 521–522.
8 G. C. O'Keeffe, *et al.*, Dopamine-induced proliferation of adult neural precursor cells in the mammalian subventricular zone is mediated through EGF, *Proc. Natl. Acad. Sci. U. S. A.*, 2009, **106**(21), 8754–8759.
9 M. Garcia-Garrote, *et al.*, Dopamine regulates adult neurogenesis in the ventricular-subventricular zone via dopamine D3 angiotensin type 2 receptor interactions, *Stem Cells*, 2021, **39**(12), 1778–1794.
10 F. Klempin, H. Babu, D. D. Tonelli, E. Alarcon, K. Fabel and G. Kempermann, Oppositional effects of serotonin receptors 5-HT1a, 2, and 2c in the regulation of adult hippocampal neurogenesis, *Front. Mol. Neurosci.*, 2010, **3**, 14.
11 E. Gould, Serotonin and hippocampal neurogenesis, *Neuropsychopharmacology*, 1999, **21**(1), 46–51.
12 N. Alenina and F. Klempin, The role of serotonin in adult hippocampal neurogenesis, *Behav. Brain Res.*, 2015, **277**, 49–57.
13 F. Klempin, *et al.*, Serotonin is required for exercise-induced adult hippocampal neurogenesis, *J. Neurosci.*, 2013, **33**(19), 8270–8275.
14 E. Hedlund, *et al.*, Dopamine receptor antagonists enhance proliferation and neurogenesis of midbrain Lmx1a-expressing progenitors, *Sci. Rep.*, 2016, **6**(1), 1–11.
15 A. Borta and G. U. Höglinger, Dopamine and adult neurogenesis, *J. Neurochem.*, 2007, **100**(3), 587–595.
16 T. Hagg, From neurotransmitters to neurotrophic factors to neurogenesis, *Neuroscientist*, 2009, **15**(1), 20–27.
17 Y. Wang, *et al.*, Human brain organoid-on-a-chip to model prenatal nicotine exposure, *Lab Chip*, 2018, **18**(6), 851–860.
18 T. Osaki, V. Sivathanu and R. D. Kamm, Engineered 3D vascular and neuronal networks in a microfluidic platform, *Sci. Rep.*, 2018, **8**(1), 1–13.
19 B. Peng, *et al.*, Blood–brain barrier (BBB)-on-a-chip: a promising breakthrough in brain disease research, *Lab Chip*, 2022, **22**(19), 3579–3602.
20 R. Mittal, *et al.*, Organ-on-chip models: implications in drug discovery and clinical applications, *J. Cell. Physiol.*, 2019, **234**(6), 8352–8380.
21 Y. Fan, *et al.*, Engineering a brain cancer chip for high-throughput drug screening, *Sci. Rep.*, 2016, **6**(1), 1–12.
22 D. Pamies, T. Hartung and H. T. Hogberg, Biological and medical applications of a brain-on-a-chip, *Exp. Biol. Med.*, 2014, **239**(9), 1096–1107.
23 O. Kilic, *et al.*, Brain-on-a-chip model enables analysis of human neuronal differentiation and chemotaxis, *Lab Chip*, 2016, **16**(21), 4152–4162.
24 J. Park, *et al.*, Three-dimensional brain-on-a-chip with an interstitial level of flow and its application as an in vitro model of Alzheimer's disease, *Lab Chip*, 2015, **15**(1), 141–150.
25 R. Yang, *et al.*, A microfluidic chip for growth and characterization of adult rat hippocampal progenitor cell neurospheroids, *J. Microelectromech. Syst.*, 2021, **31**(1), 37–44.
26 R. Yang, *et al.*, Studies of neurospheres cultured using adult hippocampal progenitor cells under off-chip magnetic stimulation, in *2019 20th International Conference on Solid-State Sensors, Actuators and Microsystems & Eurosensors XXXIII (TRANSDUCERS & EUROSENSORS XXXIII)*, IEEE, 2019, pp. 756–759.
27 F. H. Gage, Mammalian neural stem cells, *Science*, 2000, **287**(5457), 1433–1438.
28 S. Jessberger and F. H. Gage, Fate plasticity of adult hippocampal progenitors: biological relevance and therapeutic use, *Trends Pharmacol. Sci.*, 2009, **30**(2), 61–65.
29 K. T. Nguyen and J. L. West, Photopolymerizable hydrogels for tissue engineering applications, *Biomaterials*, 2002, **23**(22), 4307–4314.
30 J. Zhu, Bioactive modification of poly (ethylene glycol) hydrogels for tissue engineering, *Biomaterials*, 2010, **31**(17), 4639–4656.
31 S. Pradhan, *et al.*, PEG-fibrinogen hydrogels for three-dimensional breast cancer cell culture, *J. Biomed. Mater. Res., Part A*, 2017, **105**(1), 236–252.
32 R. M. Rounds, *et al.*, Microporated PEG spheres for fluorescent analyte detection, *J. Fluoresc.*, 2007, **17**(1), 57–63.
33 K. J. Son, *et al.*, Detecting cell-secreted growth factors in microfluidic devices using bead-based biosensors, *Microsyst. Nanoeng.*, 2017, **3**(1), 1–9.
34 R. Russell, *et al.*, Mass transfer in rapidly photopolymerized poly (ethylene glycol) hydrogels used for chemical sensing, *Polymer*, 2001, **42**(11), 4893–4901.
35 C. Khoury, *et al.*, Tunable microfabricated hydrogels—A study in protein interaction and diffusion, *Biomed. Microdevices*, 2003, **5**(1), 35–45.
36 Y. B. Gianchandani, O. Tabata and H. P. Zappe, *Comprehensive microsystems*, Elsevier Amsterdam, 2008, vol. 1.
37 J. Oh, *et al.*, Multipotent adult hippocampal progenitor cells maintained as neurospheres favor differentiation toward glial lineages, *Biotechnol. J.*, 2014, **9**(7), 921–933.
38 C. Hajal, *et al.*, Engineered human blood–brain barrier microfluidic model for vascular permeability analyses, *Nat. Protoc.*, 2022, **17**(1), 95–128.
39 M. W. van Der Helm, *et al.*, Microfluidic organ-on-chip technology for blood-brain barrier research, *Tissue Barriers*, 2016, **4**(1), e1142493.
40 M. Bonakdar, P. Graybill and R. Davalos, A microfluidic model of the blood–brain barrier to study permeabilization by pulsed electric fields, *RSC Adv.*, 2017, **7**(68), 42811–42818.
41 Y. Li, *et al.*, Study of the neurotoxicity of indoor airborne nanoparticles based on a 3D human blood-brain barrier chip, *Environ. Int.*, 2020, **143**, 105598.
42 M. Senel, *et al.*, Electrochemical micropyramid array-based sensor for in situ monitoring of dopamine released from neuroblastoma cells, *Anal. Chem.*, 2020, **92**(11), 7746–7753.

43 O. E. Fayemi, A. S. Adekunle and E. E. Ebenso, Electrochemical determination of serotonin in urine samples based on metal oxide nanoparticles/MWCNT on modified glassy carbon electrode, *Sens. Bio-Sens. Res.*, 2017, **13**, 17–27.

44 M. T. Raimondi, D. Albani and C. Giordano, An organ-on-a-chip engineered platform to study the microbiota–gut–brain axis in neurodegeneration, *Trends Mol. Med.*, 2019, **25**(9), 737–740.

45 I. Raimondi, *et al.*, Organ-on-a-chip in vitro models of the brain and the blood-brain barrier and their value to study the microbiota-gut-brain axis in neurodegeneration, *Front. Bioeng. Biotechnol.*, 2020, **7**, 435.

46 J. N. Martinson and S. T. Walk, Escherichia coli residency in the gut of healthy human adults, *EcoSal Plus*, 2020, **9**(1), DOI: **10.1128/ecosalplus.ESP-0003-2020**.

47 E. Fordjour, *et al.*, Metabolic engineering of Escherichia coli BL21 (DE3) for de novo production of L-DOPA from D-glucose, *Microb. Cell Fact.*, 2019, **18**(1), 1–10.

48 S. Ham, *et al.*, Gamma aminobutyric acid (GABA) production in Escherichia coli with pyridoxal kinase (pdxY) based regeneration system, *Enzyme Microb. Technol.*, 2022, **155**, 109994.

49 M. Park, *et al.*, Conversion of 5-hydroxytryptophan into serotonin by tryptophan decarboxylase in plants, Escherichia coli, and yeast, *Biosci., Biotechnol., Biochem.*, 2008, **72**(9), 2456–2458.

50 S. Park, *et al.*, Production of serotonin by dual expression of tryptophan decarboxylase and tryptamine 5-hydroxylase in Escherichia coli, *Appl. Microbiol. Biotechnol.*, 2011, **89**(5), 1387–1394.